Abolished $InsP_3R2$ function inhibits sweat secretion in both humans and mice

Joakim Klar,[1] Chihiro Hisatsune,[2] Shahid M. Baig,[3] Muhammad Tariq,[3] Anna C.V. Johansson,[1] Mahmood Rasool,[4] Naveed Altaf Malik,[3] Adam Ameur,[1] Kotomi Sugiura,[2] Lars Feuk,[1] Katsuhiko Mikoshiba,[2] and Niklas Dahl[1]

[1]Department of Immunology, Genetics, and Pathology, Science for Life Laboratory, Uppsala University, Uppsala, Sweden. [2]Laboratory for Developmental Neurobiology, RIKEN Brain Science Institute, Saitama, Japan. [3]Human Molecular Genetics Laboratory, National Institute for Biotechnology and Genetic Engineering (NIBGE), Faisalabad, Pakistan. [4]Center of Excellence in Genomic Medicine Research, King Abdulaziz University, Jeddah, Saudi Arabia.

There are 3 major sweat-producing glands present in skin; eccrine, apocrine, and apoeccrine glands. Due to the high rate of secretion, eccrine sweating is a vital regulator of body temperature in response to thermal stress in humans; therefore, an inability to sweat (anhidrosis) results in heat intolerance that may cause impaired consciousness and death. Here, we have reported 5 members of a consanguineous family with generalized, isolated anhidrosis, but morphologically normal eccrine sweat glands. Whole-genome analysis identified the presence of a homozygous missense mutation in *ITPR2*, which encodes the type 2 inositol 1,4,5-trisphosphate receptor ($InsP_3R2$), that was present in all affected family members. We determined that the mutation is localized within the pore forming region of $InsP_3R2$ and abrogates Ca^{2+} release from the endoplasmic reticulum, which suggests that intracellular Ca^{2+} release by $InsP_3R2$ in clear cells of the sweat glands is important for eccrine sweat production. *Itpr2*$^{-/-}$ mice exhibited a marked reduction in sweat secretion, and evaluation of sweat glands from *Itpr2*$^{-/-}$ animals revealed a decrease in Ca^{2+} response compared with controls. Together, our data indicate that loss of $InsP_3R2$-mediated Ca^{2+} release causes isolated anhidrosis in humans and suggest that specific $InsP_3R$ inhibitors have the potential to reduce sweat production in hyperhidrosis.

Introduction

Anhidrosis, defined as the absence of perspiration in the presence of an appropriate stimulus such as heat, exercise, or pharmacological agonists, is a rare condition that may be acquired or congenital (1, 2). The causes of anhidrosis or reduced sweating (hypohidrosis), which are heterogeneous, include sweat gland innervation defects (in disorders of the autonomous nervous system) and reduced number of functional sweat glands (in different ectodermal syndromes) (2). Reports of generalized and isolated anhidrosis with normal sweat glands (OMIM 106190) are very few (3, 4).

There are 3 types of sweat glands present in the skin: eccrine, apocrine, and apoeccrine. Of these, eccrine sweat glands have a superior maximum secretion rate (5, 6). Among mammals, humans have the highest proportion of eccrine sweat glands, which provides an advantage for thermal cooling during prolonged exercise (6). The eccrine gland consists of 2 major parts, the excretory duct and the secretory coil. The excretory duct has 2 or 3 layers of epithelial cells and consists of a straight portion leading to the skin surface and a coiled reabsorptive portion. The secretory portion consists of 3 functionally distinct cell types: granulated (dark) cells, parietal (clear) cells, and myoepithelial cells (6, 7). Upon initial stimulation of clear cells of the sweat gland by acetylcholine, intracellular [Ca^{2+}] increases and initiates a stepwise process leading to net loss of Na^+, Cl^-, and water into the glandular lumen (8).

The present study was undertaken to clarify the pathophysiological mechanisms behind isolated generalized anhidrosis in 5 members of a consanguineous Pakistani family. The segregation of the disease was suggestive of autosomal-recessive inheritance. A genome-wide search for the causative mutation revealed a candidate missense mutation for anhidrosis in *ITPR2*, which encodes inositol 1,4,5-trisphosphate receptor 2 ($InsP_3R2$), a Ca^{2+} release channel in the endoplasmic reticulum (9–11). We also found that loss of *Itpr2* in mice (12) resulted in markedly reduced eccrine sweat production in paws. Together, our findings indicate that loss of $InsP_3R2$-mediated Ca^{2+} release causes reduced sweat production and thus underlies isolated anhidrosis in the individuals investigated herein.

Results

Phenotype of affected family members. The available family members (n = 10) consisted of 5 affected individuals (aged 4, 5, 7, 10, and 11 years at time of study), 2 healthy siblings, and 3 parents (Figure 1A). Upon clinical investigation, no abnormal symptoms were observed or reported from family members beyond anhidrosis and severe heat intolerance. In the affected family members, body growth as well as teeth, hair, nails, and skin were normal. Biochemical analysis of serum and urine in affected family members VII:4 and VII:5 (aged 11 and 10 years, respectively) revealed electrolyte levels (Na^+, K^+, Ca^{2+}, Mg^{2+}, and Cl^-) within normal ranges. S-amylase levels were also normal. Starch-iodine sweat test (6) confirmed the absence of sweating in affected individuals, and all 5 exhibited abnormal increases in skin and ear canal temperature when exposed to heat (45°C, 45% humidity), accompanied by an abnormal increase in heart rate (Figure 1, B and C). Skin biopsy

Authorship note: Joakim Klar and Chihiro Hisatsune contributed equally to this work.
Conflict of interest: The authors have declared that no conflict of interest exists.
Submitted: May 8, 2013; **Accepted:** September 11, 2014.
Reference information: *J Clin Invest*. 2014;124(11):4773–4780. doi:10.1172/JCI70720.

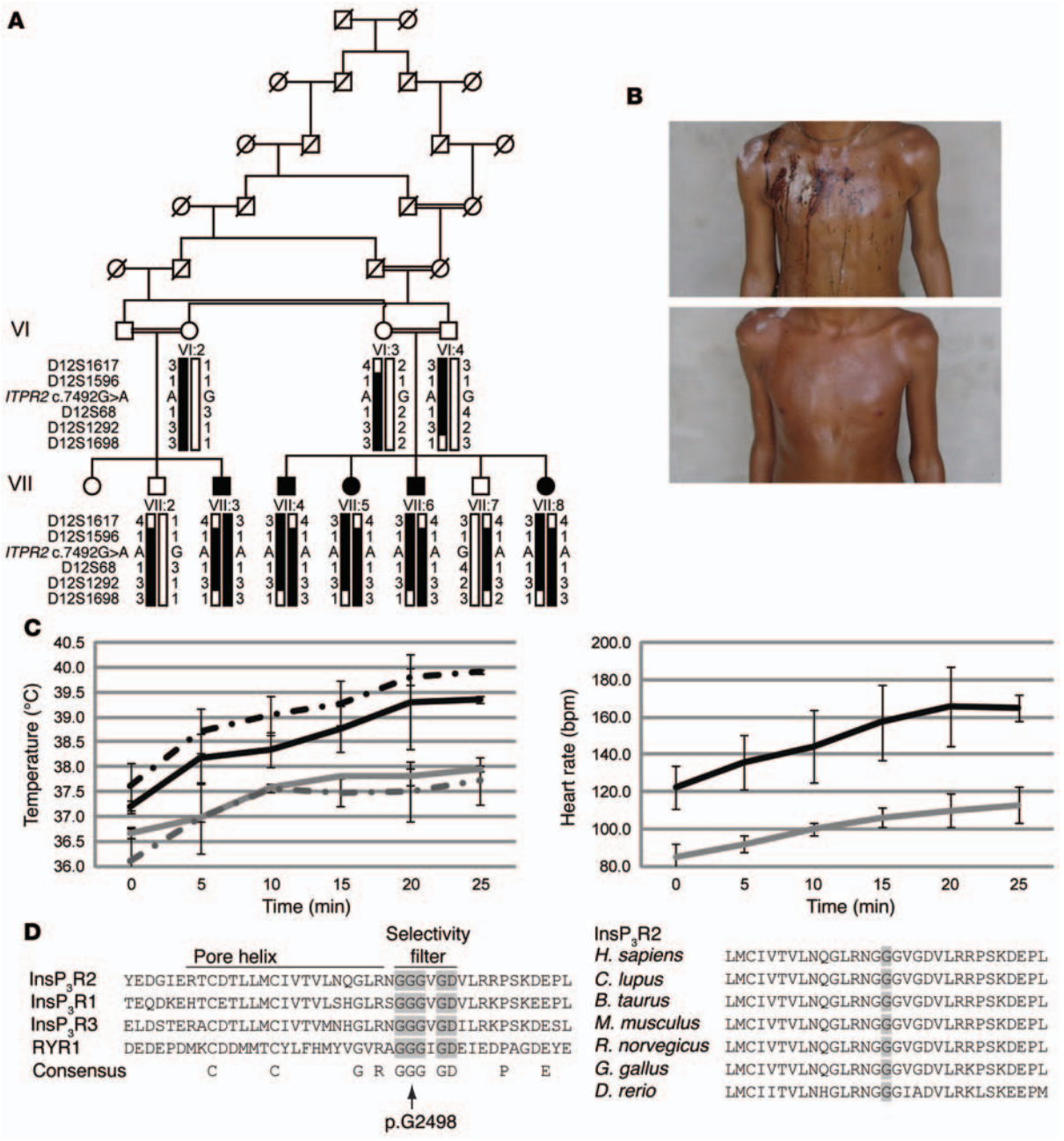

Figure 1. Genetic analysis, clinical investigation, and $InsP_3R$ sequences. (**A**) Pedigree of the consanguineous family segregating isolated anhidrosis (black symbols). Affected individuals were homozygous for chromosome 12p marker alleles flanking *ITPR2* (black bars). (**B**) Starch-iodine sweat test at 32°C, demonstrating sweating in a healthy control male (top) and absence of color (due to dry skin) in affected family member VII:4 with anhidrosis (bottom). Both subjects were 11 years of age. (**C**) Increased temperatures (left; dashed lines, skin surface; solid lines, ear canal) and heart rates (right) at rest over 25 minutes when exposed to 45°C and 45% humidity, in patients (n = 5; black lines) compared with age-matched controls (n = 3; gray lines). $P < 0.05$; Student's 2-tailed t test. (**D**) Left: Protein sequence alignment of the pore region of $InsP_3R1$–$InsP_3R3$ and RYR1. Pore helix and selectivity filter are indicated. Residues of the selectivity filters are highlighted in gray, with the mutated glycine residue (p.G2498) denoted (arrow). Consensus residues correspond to amino acids conserved among all 4 proteins. Right: Interspecies alignment of the pore helix and the selectivity filter domains of $InsP_3R2$ illustrated conservation of residue G2498. Data represent mean ± SD.

from the forearm of affected family member VII:4 demonstrated normal morphology and number of sweat glands.

Genetic analysis and identification of a candidate mutation. We first performed autozygosity mapping on affected individuals (13) because of the consanguinity and the likely autosomal-recessive inheritance pattern for anhidrosis within this family. The analysis revealed a single homozygous region on chromosome 12p12.1–12p11.22 in all 5 affected individuals (Figure 1A). The region consists of 427 consecutive homozygous SNPs (rs1337853–rs2349565) spanning 31 genes over 3.4 Mb (GRCh37 25,703,471–29,137,928). Segregation of the candidate homozygous region in the family was confirmed with polymorphic microsatellite markers, and linkage analysis resulted in a maximum 2-point logarithm of odds (LOD) score of 3.08.

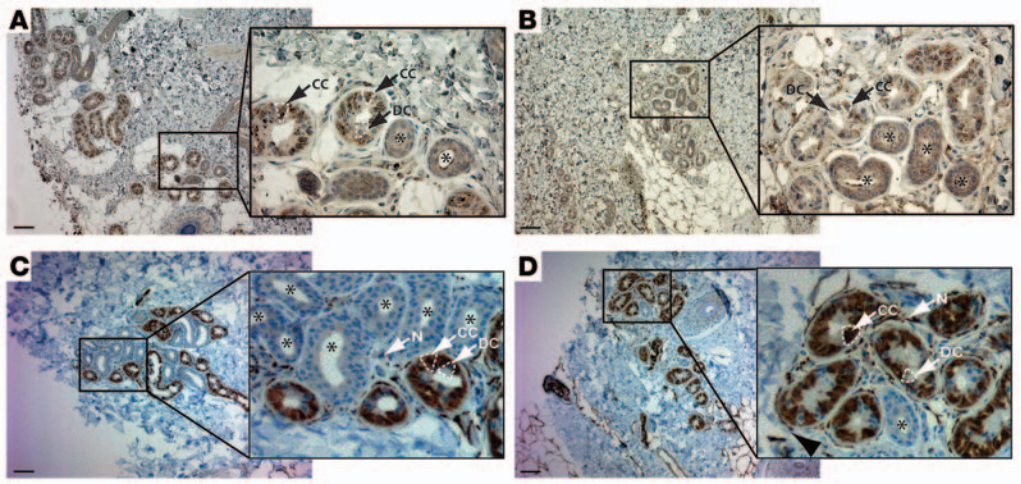

Figure 2. $InsP_3R$ immunohistochemistry in skin biopsies. (**A** and **B**) Immunoreactivity and cellular localization of $InsP_3R2$ in forearm skin biopsies of (**A**) a healthy control individual and (**B**) affected family member VII:4. Eccrine sweat glands (boxed regions) are shown enlarged. Control and patient specimens exhibited similar staining: $InsP_3R2$ stained positive in the clear cells (CC), but not the dark cells (DC) (dashed lines). $InsP_3R2$ was also present in cells of the excretory ducts (asterisk) with a concentration in subcellular regions lining the ducts. (**C** and **D**) Similar to $InsP_3R2$, S100β staining was positive in the clear cells of the secretory coil of the eccrine sweat gland, but not in the dark cells or the cells of the duct (15), in (**C**) a control individual and (**D**) affected family member VII:4. N, nerve end. Original magnification, ×10; ×40 (enlargements). Scale bars: 20 μm.

Targeted enrichment of the 3.4-Mb candidate region was performed on genomic DNA from affected members, followed by sequencing and filtering. The analysis identified a single novel coding variant: c.7492G>A in *ITPR2* (NM_002223.2). The transition results in a predicted glycine-to-serine (p.G2498S) substitution, and it was present in a homozygous state in the 5 affected family members and in a heterozygous state in the 3 parents and 2 healthy siblings available for sampling (Supplemental Figure 1; supplemental material available online with this article; doi:10.1172/JCI70720DS1). The glycine residue is highly conserved along the phylogenic scale from human to zebrafish (PhyloP score, 2.44645; GERP score, 4.43) among the 3 $InsP_3R$ subtypes as well as in the closely related ryanodine receptor 1 (RYR1; Figure 1D and ref. 10). The variant — predicted to affect protein function by PolyPhen-2 analysis (HumVar score, 1.00, probably damaging) (14) — was not found in 200 Swedish and 200 Pakistani control chromosomes, nor in 850 exomes that were available in house. Furthermore, the c.7492G>A variant is not present in the latest Exome Variant Server data release (ESP6500SI-V2; http://evs.gs.washington.edu/EVS/).

$InsP_3R$ immunohistochemistry in skin biopsies. Histology of a punch biopsy from the forearm of an affected family member confirmed normal morphology and number of sweat glands. Immunostaining of $InsP_3R2$ was positive in the clear cells of the secretory coil of the eccrine sweat gland and was similar between control and patient samples (Figure 2, A and B). In addition, $InsP_3R2$ expression was observed within the cells of the excretory duct and with a concentration in subcellular regions lining the ducts. To investigate the expression of the other $InsP_3R$ isoforms in eccrine sweat glands, we stained the skin biopsies for $InsP_3R1$ and $InsP_3R3$. Whereas $InsP_3R3$ showed weak staining in the secretory part and a strong staining in the basal (peripheral) cell layer of the excretory duct (Supplemental Figure 2), we could not detect $InsP_3R1$. Thus, both $InsP_3R2$ and $InsP_3R3$ stained positive in the secretory portion, but with somewhat complementary distributions in the excretory duct. We also stained skin biopsies for S100β, a member of the S100 protein family of Ca^{2+} binding proteins believed to be a secondary messenger in the Ca^{2+}-dependent regulatory pathway for sweat secretion (15). Similar to $InsP_3R2$, S100β was expressed in the clear cells of the eccrine secretory coil, but not in the dark cells or the cells of the duct (Figure 2, C and D).

G2498S mutation abolished the Ca^{2+} channel activity of $InsP_3R2$. To clarify the functional consequence of the $InsP_3R2$ missense mutation p.G2498S, we stably expressed WT and mutant $InsP_3R2$ in DT40 chicken B lymphocytes lacking endogenous $InsP_3Rs$ (R23-11 cells) (16) and examined their channel properties by Ca^{2+} imaging. We established 3 independent cell lines expressing WT or mutated $InsP_3R2$ and confirmed the expression of $InsP_3R2$ protein in each stable cell line (Figure 3A). We then stimulated the cells with anti-IgM antibody to activate B cell receptors and intracellular Ca^{2+} release. In response to IgM stimulation, approximately 80% of cells expressing WT $InsP_3R2$ showed intracellular Ca^{2+} oscillations (n = 139; Figure 3B), the typical form of $InsP_3R2$-mediated Ca^{2+} release, consistent with previous studies (17). In contrast, cells expressing p.G2498S mutant $InsP_3R2$ had no detectable Ca^{2+} response after IgM stimulation (n = 50; Figure 3B). The Ca^{2+} contents within the endoplasmic reticulum, as measured by passive Ca^{2+} release after Ca^{2+} pump inhibitor cyclopiazonic acid (CPA) treatment, were similar in cells expressing WT and p.G2498S mutant $InsP_3R2$ (WT, 100% ± 20.72%, n = 3; p.G2498S, 129.97% ± 55.22%, n = 3; mean ± SD; P = NS, t test). These data strongly suggest that the p.G2498S mutation causes $InsP_3R2$ loss of function.

$Itpr2^{-/-}$ mice exhibit hypohidrosis. To further examine the contribution of $InsP_3R2$ to sweat production, we examined sweat secretion in $Itpr2^{-/-}$ mice, which harbor a targeted disruption of *Itpr2*, using the starch-iodine assay (18). When pilocarpine was subcutaneously injected into the hind paws of $Itpr2^{+/+}$ mice, individual sweat glands (represented by black dots) appeared within 1 minute, and the number increased in a time-dependent manner, to 78.33 ± 10.92 dots per paw at 20 minutes (mean ± SEM, n = 7; Figure 4A). In $Itpr2^{-/-}$ mice, however, the increase in sweat gland number was significantly attenuated (24.4 ± 2.11 dots per paw at 20 minutes, n = 5; Figure 4A). In addition, the size of each black dot (presumably representing the sweat volume from a single gland) was about half the size in $Itpr2^{-/-}$ versus $Itpr2^{+/+}$ mice (Figure 4B). Similar to our analysis of human sweat glands, immunofluores-

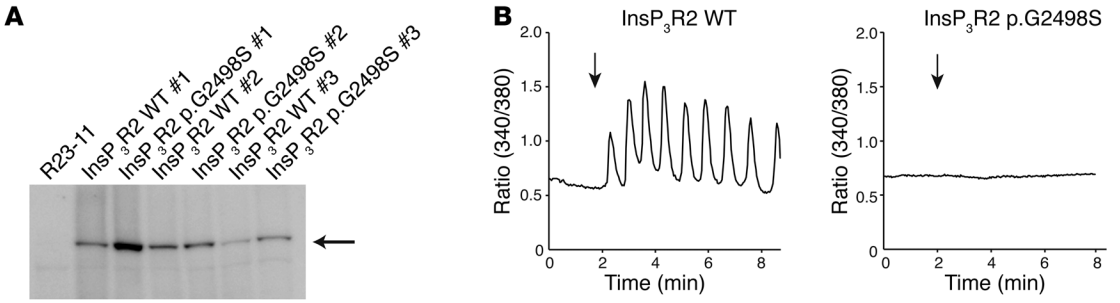

Figure 3. The p.G2498S mutation abolishes the channel activity of $InsP_3R2$. (**A**) Expression of WT and mutant p.G2498S mouse $InsP_3R2$ in 3 independent stable clones. (**B**) Intracellular Ca^{2+} signals upon IgM stimulation in R23-11 cells expressing WT and p.G2498S mouse $InsP_3R2$ variants. Arrows denote IgM stimulation (M4) at 0.25 μg/ml. Ca^{2+} signals from 2 independent p.G2498S $InsP_3R2$ clones and 1 WT $InsP_3R2$ clone were analyzed. Representative data (ratio change of Fura-2) from 4 independent experiments are shown. Cells expressing p.G2498S $InsP_3R2$ exhibited no detectable Ca^{2+} signal in response to IgM stimulation (0%; *n* = 50 cells). Of WT $InsP_3R2$ cells, 78% showed Ca^{2+} oscillation, 14% were Ca^{2+} transient, and 8% exhibited no response (*n* = 139 cells).

cence staining of mouse digits confirmed $InsP_3R2$ expression in S100β-expressing cells of *Itpr2*$^{+/+}$ sweat glands, which was not seen in *Itpr2*$^{-/-}$ mice (Figure 4C).

To examine Ca^{2+} signals in sweat glands, we dissected out individual sweat glands from mouse paws, loaded them with the Ca^{2+} indicators Fura Red and Fluo4, and subjected them to stimulation with various concentrations of acetylcholine. In glands from *Itpr2*$^{+/+}$ mice, we found that the amplitude of Ca^{2+} signals in the secretory part increased in a dose-dependent manner (Figure 5, A and B, and Supplemental Video 1), but there were no changes in Ca^{2+} signals in the excretory duct (Figure 5A, arrow). We then compared the peak amplitude of Ca^{2+} signals in dissected *Itpr2*$^{+/+}$ and *Itpr2*$^{-/-}$ sweat glands after acetylcholine stimulation and found an approximately 40%–50% reduction in the latter at every dose tested (Figure 5, B and C). Consistent with the reduced Ca^{2+} signals, Western blot analysis of sweat gland lysates with anti–pan-$InsP_3R$ antibody demonstrated that total $InsP_3R$ expression in *Itpr2*$^{-/-}$ sweat glands decreased to about 40% that of *Itpr2*$^{+/+}$ sweat glands (Figure 5D). Thus, the extant but reduced sweat production and the residual Ca^{2+} signals in *Itpr2*$^{-/-}$ mouse sweat glands are likely due to expression of $InsP_3R1$ and $InsP_3R3$. This was further supported by the positive immunohistochemical staining for $InsP_3R1$ and $InsP_3R3$ in the clear cells of mouse sweat glands (Supplemental Figure 3).

Discussion

The primary goal of this study was to identify the pathophysiological mechanism leading to congenital generalized and isolated anhidrosis. The study emerged from the investigation of a consanguineous family segregating autosomal-recessive anhidrosis in 5 children. The affected individuals presented with absent eccrine sweat production and with severe and congenital heat intolerance, but no other symptoms from the skin or other ectodermal tissues, such as teeth and hair. The children exhibited normal development and were otherwise healthy. Hence, the clinical picture was not compatible with an ectodermal syndrome. Skin biopsy of an affected individual confirmed normal sweat gland morphology, suggestive of a gland-intrinsic mechanism.

Genetic analysis identified a unique transition (c.7492G>A) that predicts a missense variant (p.G2498S) in *ITPR2*, which encodes $InsP_3R2$. The transition was present in a homozygous state in the affected family members and was excluded in control populations. Intracellular Ca^{2+} release in clear cells of sweat glands is a known critical event for sweat induction (15), and we thus considered the mutated $InsP_3R2$ variant to be a good candidate for the cause of anhidrosis. This hypothesis was supported by our immunostaining of sweat glands from human skin biopsies, which showed distinct expression of $InsP_3R2$ in the secretory portion and in the reabsorbing excretory duct. Both the secretory portion and the ductal part are involved in the net production of sweat; however, the epithelium lining of the sweat duct is not freely permeable to water, which indicates that ductal reabsorption has little effect on secreted sweat volume (19). The missense variant p.G2498S is localized in the pore-forming domain (Pfam, PF00520; residues 2,336–2,540) of $InsP_3R2$. More specifically, the substitution involves the second glycine in the selectivity filter formed by a core of 5 residues, GGGXG (Figure 1D and refs. 10, 20). In rat $InsP_3R1$ (type I-pore), the G2546 residue corresponds to $InsP_3R2$ G2498, and mutagenesis of $InsP_3R1$ G2546 (i.e., p.G2546A) results in inactivation of the channel activity. That is, p.G2546A mutant $InsP_3R1$ is still able to form homotetramers but unable to mediate Ca^{2+} release from microsomal vesicles, and it is nonfunctional in a Ca^{2+} flux assay (21).

We then analyzed p.G2498S mutant $InsP_3R2$ in a chicken cell system devoid of endogenous $InsP_3Rs$, and the results were consistent with a loss-of-function effect of the p.G2498S mutation. Cells expressing the p.G2498S mutant $InsP_3R2$ showed a complete loss of Ca^{2+} response upon stimulation, despite Ca^{2+} stores similar to those of control cells expressing WT $InsP_3R2$. Thus, the abolished intracellular Ca^{2+} release from the $InsP_3R2$ p.G2498S variant is consistent with previous studies on rat $InsP_3R1$ with a mutation in the corresponding residue (21).

To independently assess the role of $InsP_3R2$ in sweat production, we analyzed eccrine glands in paws of *Itpr2*$^{-/-}$ mice. We observed a 3-fold reduction in the number of pilocarpine-responsive sweat glands on *Itpr2*$^{-/-}$ mouse paws, and dissected *Itpr2*$^{-/-}$ sweat glands showed a significant reduction in Ca^{2+} response after acetylcholine stimulation compared with those of *Itpr2*$^{+/+}$ mice. Together, these results indicate that $InsP_3R2$ plays a critical role in sweat secretion in both mice and humans. However, the residual sweat production in *Itpr2*$^{-/-}$ mice is not fully consistent with the anhidrosis in the human subjects homozygous for the c.7492G>A (p.G2498S) mutation. Our immunohistochemical analysis suggests that $InsP_3R2$ and $InsP_3R3$ are the predominant isoforms expressed in human sweat glands,

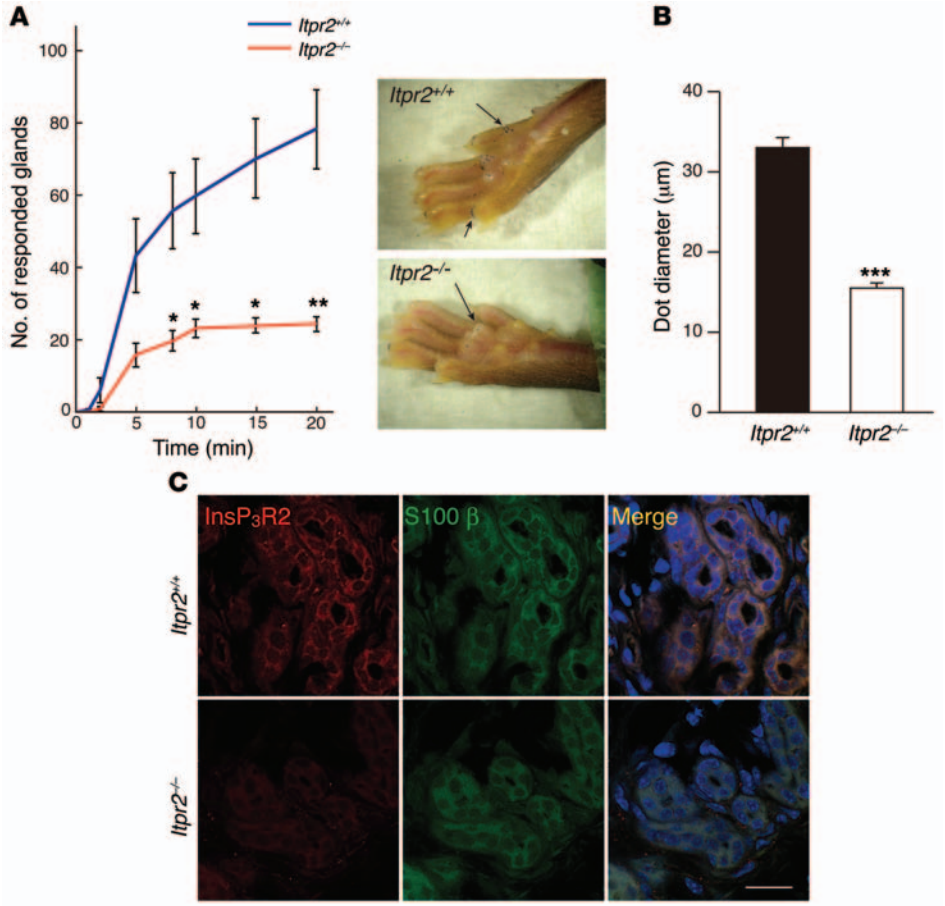

Figure 4. Decreased sweat secretion in *Itpr2*$^{-/-}$ mice. (**A**) Pilocarpine-induced sweat response in *Itpr2*$^{+/+}$ (n = 7) and *Itpr2*$^{-/-}$ (n = 5) mice visualized by the Starch-iodine assay. Representative images of *Itpr2*$^{+/+}$ and *Itpr2*$^{-/-}$ mouse paws 20 minutes after pilocarpine injection are shown. The number of black dots (arrows) was counted at the indicated times after injection. *P < 0.05, **P < 0.005, Student's 2-tailed t test. (**B**) Dot diameter 20 minutes after pilocarpine injection. (**C**) Immunohistochemistry of $InsP_3R2$ in sweat glands of *Itpr2*$^{+/+}$ and *Itpr2*$^{-/-}$ mice. Red, $InsP_3R2$; green, S100β; blue, DAPI. Data represent mean ± SEM. Scale bar: 20 μm.

and staining of skin biopsies from anhidrotic patients suggested normal levels of the mutated $InsP_3R2$ isoform in sweat glands. Although $InsP_3R2$ is required for normal sweat production in both humans and mice, the phenotypic discrepancy between our patients and the *Itpr2*$^{-/-}$ model could be explained to some extent by interspecies differences in $InsP_3R$ expression for sweat gland function. This notion was supported by immunohistochemistry showing that the $InsP_3R1$ isoform was expressed in mouse, but not human, sweat glands as well as the fact that $InsP_3R1$ contributes significantly to the peak height of Ca^{2+} signals (22). Additionally, we cannot exclude the possibility that the relative level of $InsP_3R3$ is higher in murine versus human clear cells. The expression levels of $InsP_3R1$ and $InsP_3R3$ may thus partially compensate for the loss of $InsP_3R2$ in sweat glands of the *Itpr2*$^{-/-}$ mice. However, $InsP_3R1$ is not expressed in human clear cells, and expression of $InsP_3R2$ far exceeds that of $InsP_3R3$. Therefore, one possibility is that the $InsP_3R3$ present in human patients is insufficient to compensate for the mutant $InsP_3R2$. Furthermore, the p.G2498S variant of $InsP_3R2$ may have a dominant-negative effect when forming heterotetramers with $InsP_3R3$ in humans. If $InsP_3R2$ is the predominant isoform in human clear cells, the stoichiometry of the expressed $InsP_3R$ isoforms would then result in mostly non-functional Ca^{2+} channels. However, in other tissues of the patients, the level of expressed $InsP_3R2$ mutant proteins may be insufficient to interfere with $InsP_3R1$ and $InsP_3R3$ function. Finally, the different stimuli used to provoke sweat production in the *Itpr2*$^{-/-}$ mice and human subjects may contribute to the distinct phenotypes. The more physiological induction used in human subjects (i.e., increased temperature) is not comparable to the pilocarpine injections used in mice.

Changes in intracellular [Ca^{2+}] represent a versatile signaling system regulating diverse cellular processes, including cell differentiation and an individual's metabolism (9). Different combinations of $InsP_3Rs$ are required for organ development, for heart (23) and brain (24) function, and for taste perception (25). In line with this, our present data suggest a distinct contribution of the $InsP_3R2$ isoform for exocrine function in salivary and pancreas glands versus sweat glands. Whereas *Itpr2*$^{-/-}$ mice exhibited reduced sweat production, they do not show perturbed function of the salivary and pancreatic glands (12). Similarly, the 5 affected family members herein did not present with any abnormal symptoms besides the anhidrosis and severe heat sensitivity. The affected individuals did not report on dry mouth, reduced saliva production, or malabsorption, although minor differences cannot be excluded. Moreover, the growth curves of the patients were within normal ranges. For comparison, *Itpr2*$^{-/-}$ *Itpr3*$^{-/-}$ double-knockout mice are hypoglycemic and show growth delay related to dysfunction of the pancreas and the salivary glands (12). Thus, the contribution of $InsP_3R2$ to exocrine function is likely to be different in sweat glands than in salivary and pancreatic glands, possibly resulting from variations in the relative levels of the 3 $InsP_3Rs$. Additionally, redundant function for the $InsP_3Rs$ may provide tolerance for quantitative reductions in their channel activity in distinct organs and for adequate development and functionality.

In conclusion, we identified the first mutation of $InsP_3R2$ associated with human disease. Our results demonstrated that $InsP_3R2$-mediated Ca^{2+} release plays an important role in sweat secretion in both humans and mice. Our findings indicate that the $InsP_3R2$ missense mutation p.G2498S underlies the isolated anhidrosis in 5 related patients and that lack of a functional $InsP_3R2$ compromised Ca^{2+} release, resulting in the absence of sweat production. The human phenotype was modeled in the *Itpr2*$^{-/-}$ mice, albeit with a milder phenotype corresponding to hypohidrosis. Because eccrine sweating is fundamental for thermoregulation in humans (5), we conclude that $InsP_3R2$ plays a critical role for thermal cooling. Our

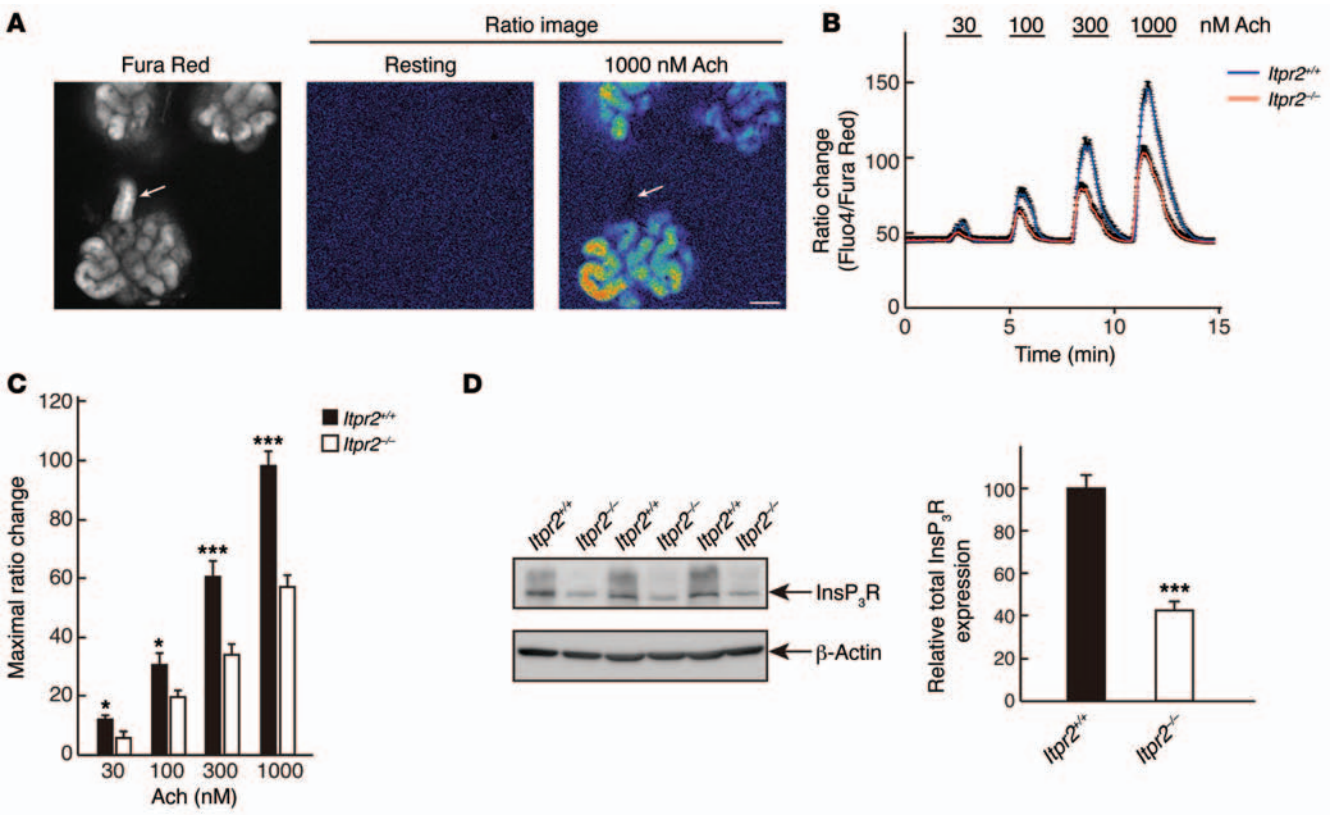

Figure 5. Decreased acetylcholine-induced Ca^{2+} response of sweat glands from *Itpr2*$^{-/-}$ mice. (**A**) Ratio change of Fluo4/Fura Red in sweat glands in response to acetylcholine stimulation. Left: Fura Red image. Arrow indicates the duct portion of a sweat gland. Right: Pseudocolored ratio images of Fluo4/Fura Red before (resting) and after stimulation with 1,000 nM acetylcholine (Ach). Scale bar: 50 μm. (**B**) Ratio change (see Methods) in sweat glands in response to various dose of acetylcholine. (**C**) Maximal ratio change (see Methods) of sweat glands (*Itpr2*$^{+/+}$, 22 glands; *Itpr2*$^{-/-}$, 27 glands) at various acetylcholine concentrations. (**D**) Expression of total $InsP_3Rs$ ($InsP_3R1$–$InsP_3R3$) in *Itpr2*$^{+/+}$ and *Itpr2*$^{-/-}$ sweat glands, detected with anti–pan-$InsP_3R$ antibody. Each lane corresponds to a sample from an individual mouse. Quantification of total $InsP_3R$ expression in *Itpr2*$^{+/+}$ and *Itpr2*$^{-/-}$ mouse sweat glands is also shown (n = 3); band intensities were normalized to β-actin. Data represent mean ± SEM. $^*P < 0.05$, $^{***}P < 0.001$, Student's t test.

findings highlight $InsP_3R2$ as a potential pharmacological target in the treatment of conditions such as hyperhydrosis.

Methods

Clinical samples. A consanguineous Pakistani family with 5 children affected by severe heat intolerance was referred to the Health Division of NIBGE. Blood and urine samples were obtained from available family members, and punch skin biopsies were taken from 2 affected individuals. Consanguinity was ascertained over several generations, and 4 full siblings and 1 first cousin segregated autosomal-recessive congenital anhidrosis and severe heat intolerance (Figure 1A).

Sequencing and sequence variant detection. SNP genotyping was performed on DNA samples from 4 affected family members, using the GeneChip Mapping 250K array (Affymetrix) according to the manufacturer's protocol. Homozygosity mapping and sorting of genomic regions were performed as described previously with the dedicated software AutoSNPa (13). A cutoff of >130 homozygous SNPs was used for selection of candidate regions. Selected regions were further investigated by genotyping all available family members with microsatellite markers. We calculated 2-point LOD scores using the MLINK program of the LINKAGE package (26), assuming autosomal-recessive inheritance, equal male/female recombination rate, full penetrance, and disease allele frequency of 0.00001. Equal allele frequencies of the genotyped markers were used in the calculations. The pedigree was drawn using Cyrillic software (version 2.1.3; Cherwell Scientific Publishing Ltd.), and haplotype analysis was performed manually. A custom enrichment design covering 7M base pairs (NimbleGen Sequence Capture Microarrays; Roche) was used to enrich for the linked region on chromosome 12 (average fold enrichment, 346). Sequencing of the enriched region was performed using the Illumina HiSeq system, and variant detection was performed using LifeScope software (version 2.1; Invitrogen). SNPs and indel data were deposited in GEO (accession no. GSE61122) and additionally stored in an in-house database together with variant annotation information obtained from dbSNP135. Prediction of possible effect on protein function was performed using PolyPhen-2 analysis (14). Exon 53 of *ITPR2* (NM_002223.2) was analyzed for the identified variant by bidirectional sequencing of genomic DNA from all available family members using sense (TTGTGTCACGGCACAATTAGA) and antisense (AAAAAGATGTGCTCCTTGAAAA) primers. Sequence reactions were generated using the BigDye Terminator v3.1 Cycle Sequencing Kit (Invitrogen) according to the manufacturer's protocol and separated on an ABI 3700 instrument (Applied Biosystems).

Immunohistochemistry. Histological analysis of skin biopsies was performed after H&E staining. Immunostaining using anti-human S100 (Z0311; Dako), $InsP_3R1$ (HPA016487; Sigma-Aldrich), $InsP_3R2$ (AB9074; Millipore), and $InsP_3R3$ (LC3; ref. 27) antibodies was performed using a DAKO autostainer (Dako). Antibodies were detected using a DAKO Chemmate EnVision kit (Dako). Specificity of the anti-

$InsP_3R1$ antibody was confirmed using Western blotting and immunocytochemistry of HeLa cells overexpressing $InsP_3R1$, $InsP_3R2$, or $InsP_3R3$ (data not shown).

Mutagenesis and expression analysis. The *Apa*I fragment (2.6 kb) from pBluescript II-C2 construct (28) was cloned into the *Apa*I site of pBluescript II. Using the plasmid as a template, p.G2498S mutagenesis was performed using sense (CAGGGCCTCAGGAATGG CAGCGGAGTTGGGGATGTGCTGAG) and antisense (CTCAGCA-CATCCCCAACTCCGCTGCCATTCCTGAGGCCCTG) primers and QuikChange Site-Directed Mutagenesis Kit (Agilent Technologies). The mutated *Apa*I fragment was replaced with the *Apa*I fragment of pBluescript II-C2 to construct pBluescript II-C2-G2498S, and the *Sal*I fragment from the vector was cloned into the *Sal*I site of pBactST-neoB. Nucleotide sequences were confirmed by DNA sequencing (Applied Biosystems). Stable clones were established by transfecting the expression vectors into R2311 cells (16), as described previously (28). For expression analysis, 5.0×10^5 cells were directly lysed with a SDS-PAGE sample buffer, separated by SDS-PAGE gel, and probed with anti-$InsP_3R2$ antibody (AB9074; Millipore) by Western blotting.

Single-cell Ca^{2+} imaging. Cells were loaded with 5 μM Fura-2/AM (Dojindo Laboratories) for 20 minutes at room temperature in RPMI (Nacalai Tesque Inc.) containing 10% bovine serum. After washing with recording solution (115 mM NaCl, 5.4 mM KCl, 1 mM $MgCl_2$, 2 mM $CaCl_2$, 20 mM HEPES, and 10 mM glucose, pH 7.42), cells were plated on 3.5-cm glass-bottomed dishes. After resting Ca^{2+} level was recorded for 2 minutes, cells were stimulated with anti-BCR antibody (M4) at 0.25 μg/ml (16). Fura-2 fluorescent images were analyzed using an inverted microscope (ECLIPSE TE300; Nikon) and a video image analysis system (Argus-50/CA; Hamamatsu Photonics) with excitation filters at 340 ± 10 and 380 ± 10 nm, a dichroic beam splitter at 400 nm, and a bandpass emission filter at 510–550 nm.

Mouse studies. *Itpr2*$^{-/-}$ mice were described previously (12). *Itpr2*$^{+/+}$ and *Itpr2*$^{-/-}$ mice (3 weeks old) were anesthetized by intraperitoneal injection of 36 mg/kg ketamine (Daiichi Sankyo) and 16 mg/kg xylazine (Bayer HealthCare). Mouse paws were painted with iodine (5.0% in ethanol; Sigma-Aldrich), then covered with starch solution (0.5 g/ml in mineral oil; Sigma-Aldrich). To measure sweat secretion, 50 μg pilocarpine was subcutaneously injected into the foot, images were taken of mouse paws over time, and the number and diameter of black dots were determined as described previously (18).

For immunohistochemistry, 5.0-μm paraffin sections of 4.0% PFA-fixed mouse paws were treated with 0.2% Triton in PBS for 5 minutes at room temperature. Sections were treated with boiled citric acid buffer for 5 minutes. After blocking with PBS containing 1.0% BSA and 3.0% skim milk for 1 hour at room temperature, tissues were stained with rabbit anti-$InsP_3R2$ antibody (1:500 dilution; AB9074; Millipore), rabbit anti-$InsP_3R3$ antibody (LC3; ref. 27), rat anti-$InsP_3R1$ antibody (4C11; ref. 29), and mouse anti-S100β antibody (1:500 dilution; Sigma-Aldrich) overnight at 4°C. After washing with PBS for 15 minutes, tissues were stained with Alexa Fluor 594–conjugated anti-rabbit IgG antibody and Alexa Fluor 488–conjugated anti-mouse IgG antibody (Invitrogen) for 60 minutes, then washed again with PBS for 15 minutes. The coverslips were mounted with Vectashield (Vector Laboratories), and signals were visualized using IX-70 confocal fluorescence microscopy (Olympus) or E600 fluorescent microscopy (Nikon).

For Ca^{2+} imaging of sweat glands, tips of mouse digits were cut with a blade, and the sweat glands seen in the cutting plane were corrected into the recording buffer using a pair of fine forceps under a stereoscopic microscope. The sweat glands were loaded with both 5 μM Fluo4/AM and 10 μM Fura Red/AM in the recording buffer for 1 hour. After washing, sweat glands were put on 3.5-cm glass dishes precoated with Cell-Tak (BD Biosciences), and the change of Fluo4 and Fura Red fluorescent signals were alternatively recorded with IX81 microscopy (Olympus), CSU-X1 (Yokogawa), SpectraX Light Engine (Lumencor), and MetaMorph software. Each sweat gland was encircled by a circular region of interest (matching the diameter of the sweat gland tube), and the peak Fluo4/Fura Red ratio change value was taken as the maximal ratio change of the sweat gland.

For immunoblotting of mouse sweat gland lysates, the corrected sweat glands from each *Itpr2*$^{+/+}$ and *Itpr2*$^{-/-}$ mouse paw were lysed with 35 μl SDS sample buffer. After centrifugation at 20,000 *g*, 15 μl of the lysate was loaded on 6.5% SDS-PAGE. The protein were transferred to PVDF membrane, blocked with PBST containing ECL advance blocking reagent (GE Healthcare), and probed with rabbit anti–pan-$InsP_3R$ antibody (22) and mouse anti–β-actin antibody (Sigma-Aldrich). After washing with PBST, the membrane was probed with HRP-conjugated anti-rabbit IgG and anti-mouse IgG antibodies. After washing with PBST, the membrane was incubated with HRP substrate, and chemiluminescent signals were developed with LAS-3000 (Fujifilm).

Statistics. Student's 2-tailed *t* test assuming equal variance was used for statistical analysis. A *P* value less than 0.05 was considered significant.

Study approval. Clinical investigations of patients and family members, sweat tests, temperature measurements, and skin biopsies were carried out in accordance with the Declaration of Helsinki, and the study protocol was approved by the ethics committee of NIBGE. All participating family members and their legal guardians provided written informed consent. Animal studies were approved by the review board at RIKEN Brain Science Institute, and all animals were treated according to the ethical guidelines of the Animal Experiments Committee of RIKEN Brain Science Institute.

Acknowledgments

This work was supported in part by the Swedish Research Council (K2013-66X-10829-20-3 and 621-2009-4629) and Swedish Links, Asia (348-2008-6069); Science for Life laboratory Uppsala University and Uppsala University Hospital; Grants-in-Aid for Scientific Research (20220007, to K. Mikoshiba; 24500451, to C. Hisatsune); and The Moritani Scholarship Foundation (to C. Hisatsune). J. Klar is supported by the Swedish Society for Medical Research. We thank all family members who participated in this study. We also thank C. Yokoyama and A.V. Terashima for fruitful discussions; M.W. Sherwood, A. Miyamoto, E. Ebisui, and N. Ogawa for experimental advice and help; all staff of the Support Unit for Bio-Material Analysis RIKEN BSI Research Resources Center; and the Uppsala Genome Center for technical support.

Address correspondence to: Niklas Dahl, Department of Immunology, Genetics and Pathology, Science for Life Laboratory, Uppsala University, BMC, Box 815, 751 08 Uppsala, Sweden. Phone: 46.18.4714859; E-mail: niklas.dahl@igp.uu.se. Or to: Katsuhiko Mikoshiba, Laboratory for Developmental Neurobiology, RIKEN Brain Science Institute, 2-1 Hirosawa, Wako City 351-0198, Japan. Phone: 81.48.467.9745; E-mail: mikosiba@brain.riken.jp.

1. Quinton PM. Sweating and its disorders. *Annu Rev Med*. 1983;34:429–452.
2. Sato K, Kang WH, Saga K, Sato KT. Biology of sweat glands and their disorders. II. Disorders of sweat gland function. *J Am Acad Dermatol*. 1989;20(5):713–726.
3. Dann EJ, Epstein Y, Sohar E. Familial generalized anhidrosis. *Isr J Med Sci*. 1990;26(8):451–453.
4. Armah DB, Al-Khenaizan S, Wakeel AA. Isolated Simple Anhidrosis: A rare cause of fever of unknown origin. *Curr Pediatr Res*. 2009;13(1–2):13.
5. Folk GE, Folk GE Jr, Semken HA, Semken HA Jr. The evolution of sweat glands. *Int J Biometeorol*. 1991;35(3):180–186.
6. Wilke K, Martin A, Terstegen L, Biel SS. A short history of sweat gland biology. *Int J Cosmet Sci*. 2007;29(3):169–179.
7. Zancanaro C, Merigo F, Crescimanno C, Orlandini S, Osculati A. Immunohistochemical evidence suggests intrinsic regulatory activity of human eccrine sweat glands. *J Anat*. 1999;194(pt 3):433–444.
8. Sato K, Sato F. Pharmacologic responsiveness of isolated single eccrine sweat glands. *Am J Physiol*. 1981;240(1):R44–R51.
9. Berridge MJ, Irvine RF. Inositol trisphosphate, a novel second messenger in cellular signal transduction. *Nature*. 1984;312(5992):315–321.
10. Foskett JK, White C, Cheung KH, Mak DO. Inositol trisphosphate receptor Ca^{2+} release channels. *Physiol Rev*. 2007;87(2):593–658.
11. Mikoshiba K. IP3 receptor/Ca^{2+} channel: from discovery to new signaling concepts. *J Neurochem*. 2007;102(5):1426–1446.
12. Futatsugi A, et al. IP3 receptor types 2 and 3 mediate exocrine secretion underlying energy metabolism. *Science*. 2005;309(5744):2232–2234.
13. Carr IM, Flintoff KJ, Taylor GR, Markham AF, Bonthron DT. Interactive visual analysis of SNP data for rapid autozygosity mapping in consanguineous families. *Hum Mutat*. 2006;27(10):1041–1046.
14. Adzhubei IA, et al. A method and server for predicting damaging missense mutations. *Nat Methods*. 2010;7(4):248–249.
15. Sato K, Kang WH, Saga K, Sato KT. Biology of sweat glands and their disorders. I. Normal sweat gland function. *J Am Acad Dermatol*. 1989;20(4):537–563.
16. Sugawara H, Kurosaki M, Takata M, Kurosaki T. Genetic evidence for involvement of type 1, type 2, and type 3 inositol 1,4,5-trisphosphate receptors in signal transduction through the B-cell antigen receptor. *EMBO J*. 1997;16(11):3078–3088.
17. Miyakawa T, Maeda A, Yamazawa T, Hirose K, Kurosaki T, Iino M. Encoding of Ca^{2+} signals by differential expression of IP3 receptor subtypes. *EMBO J*. 1999;18(5):1303–1308.
18. Tafari AT, Thomas SA, Palmiter RD. Norepinephrine facilitates the development of the murine sweat response but is not essential. *J Neurosci*. 1997;17(11):4275–4281.
19. Mangos J. Transductal fluxes of Na, K, and water in the human eccrine sweat gland. *Am J Physiol*. 1973;224(5):1235–1240.
20. Yule DI, Betzenhauser MJ, Joseph SK. Linking structure to function: recent lessons from inositol 1,4,5-trisphosphate receptor mutagenesis. *Cell Calcium*. 2010;47(6):469–479.
21. Schug ZT, et al. Molecular characterization of the inositol 1,4,5-trisphosphate receptor pore-forming segment. *J Biol Chem*. 2008;283(5):2939–2948.
22. Hattori M, et al. Distinct roles of inositol 1,4,5-trisphosphate receptor types 1 and 3 in Ca^{2+} signaling. *J Biol Chem*. 2004;279(12):11967–11975.
23. Uchida K, et al. Gene knock-outs of inositol 1,4,5-trisphosphate receptors types 1 and 2 result in perturbation of cardiogenesis. *PLoS One*. 2010;5(9):e12500.
24. Matsumoto M, et al. Ataxia and epileptic seizures in mice lacking type 1 inositol 1,4,5-trisphosphate receptor. *Nature*. 1996;379(6561):168–171.
25. Hisatsune C, et al. Abnormal taste perception in mice lacking the type 3 inositol 1,4,5-trisphosphate receptor. *J Biol Chem*. 2007;282(51):37225–37231.
26. Lathrop GM, Lalouel JM. Easy calculations of lod scores and genetic risks on small computers. *Am J Hum Genet*. 1984;36(2):460–465.
27. Sato-Miyaoka M, Hisatsune C, Ebisui E, Ogawa N, Takahashi-Iwanaga H, Mikoshiba K. Regulation of hair shedding by the type 3 IP3 receptor. *J Invest Dermatol*. 2012;132(9):2137–2147.
28. Iwai M, et al. Molecular cloning of mouse type 2 and type 3 inositol 1,4,5-trisphosphate receptors and identification of a novel type 2 receptor splice variant. *J Biol Chem*. 2005;280(11):10305–10317.
29. Maeda N, Niinobe M, Nakahira K, Mikoshiba K. Purification and characterization of P400 protein, a glycoprotein characteristic of Purkinje cell, from mouse cerebellum. *J Neurochem*. 1988;51(6):1724–1730.